Available online at www.sciencedirect.com
ScienceDirect
Journal of Photochemistry and Photobiology A: Chemistry 187 (2007) 363–369
Journal of Photochemistry and Photobiology A:Chemistry
www.elsevier.com/locate/jphotochem

Shape, size and photocatalytic activity control of TiO_2 nanoparticles with surfactants

D.L. Liao, B.Q. Liao *

Department of Chemical Engineering, Lakehead University, 955 Oliver Road, Thunder Bay, ON, Canada P7B 5E1

Received 3 August 2006; received in revised form 1 November 2006; accepted 6 November 2006
Available online 9 November 2006

Abstract

Shape-, size- and photocatalytic activity-controlled TiO_2 nanoparticles were prepared from $Ti(OBu)_4$ and $TiCl_4$ through the sol–gel method and studied for photocatalytic decomposition of methyl orange in fixed film batch reactors. The results showed that shape and size of TiO_2 nanoparticles could be manipulated by the use of surfactants during preparation. Spherical, cubic, ellipse nanoparticles and nanorods of TiO_2 were obtained with different surfactants. Shape- and size-controlled TiO_2 nanoparticles showed a red shift in UV–vis light reflectance spectra, which would be beneficial for photocatalytic reactions, as compared to TiO_2 nanoparticles obtained without the use of surfactants. TiO_2 nanoparticles with different shapes and sizes showed different photocatalytic activities. Cubic nanoparticles prepared with the use of sodium dodecyl sulfate had a higher photocatalytic activity than other TiO_2 nanoparticles.

Keywords: TiO_2 nanoparticle; Sol–gel; Shape-controlled nanoparticle; Size-controlled nanoparticle; Surfactant; Photocatalytic activity

1. Introduction

Control of shape and size of nanoparticles is of significant importance in catalytic reactions [1]. A number of studies have shown that catalytic activity of nanoparticles depends on not only their sizes [2–6] but also their shapes [7–13]. In addition, an extension of the wavelength range of light absorption of TiO_2 nanoparticles increased its photocatalytic activity [14].

Many studies have described the shape and size control of inorganic nanoparticles by using conventional synthesis methods such as the sol–gel method, hydrothermal method, molecular beam expitaxy and metal-organic chemical vapor deposition [7,8]. Controlling the shape and size of inorganic nanoparticles with the introduction of surfactants has been recently developed [14]. A number of different shapes, including rod-, arrow-, teardrop-, tetrapod- and disk-shape, of nanoparticles were prepared by introducing surfactants during preparation [15–17].

Due to their large surface area and high catalytic activity, great interest has been addressed to TiO_2 nanoparticles as an important photocatalyst [16]. Lots of studies on photocatalystic decomposition of organic pollutants by using TiO_2 nanoparticles have been reported in recent years [17–21]. Various shapes of TiO_2 nanocrystals, such as short and long nanorods, bullet- and diamond-shaped nanoparticles, nanotubes, cuboids and fractals have been prepared through different processes [22]. The photocatalytic activity of mesoporous TiO_2 films has been found to be higher than that of conventional anatase TiO_2 films because light harvesting can be enhanced due to the enlarged surface area and multiple scattering [23]. Mesoporous TiO_2 nanoparticles or films are often prepared by sol–gel method with the presence of surfactants [24], solvothermal method [25], co-polymer template methods [26] and low-temperature-sintered method [27]. Furthermore, the mesopores can also facilitate better accessibility of reactants to the catalysts [28]. However, some studies found that the photocatalytic activity of structured mesoporous TiO_2 is lower than the commercial photocatalyst Degussa P-25 [29].

In a summary, these studies suffered from a lack of fundamental understanding of the relationship between structure and function. Therefore, optimal conditions and/or structure for a higher photocatalytic activity of TiO_2 nanoparticles are not well understood yet. In this study, we report the shape and size control of TiO_2 nanoparticles by using a relatively new approach

* Corresponding author. Tel.: +1 807 343 8437; fax: +1 807 343 8928.
E-mail address: bliao@lakeheadu.ca (B.Q. Liao).

1010-6030/$ – see front matter © 2006 Elsevier B.V. All rights reserved.
doi:10.1016/j.jphotochem.2006.11.003

of introducing surfactants during preparation. Through shape and size control, photocatalytic activity was manipulated and improved.

2. Experiments

2.1. Chemicals

Titanium butoxide ($Ti(OBu)_4$, 97%), titanium chloride ($TiCl_4$, 99%), ammonium hydroxide, ethanol, sodium dodecyl benzene sulfonate (DBS), sodium dodecyl sulfate (SDS) and hydroxypropyl methyl cellulose were purchased from Sigma–Aldrich Ltd. without further purification. Double distilled and deionized water was used throughout in this research.

2.2. Experiment

TiO_2 nanoparticles were obtained through the hydrolysis of titanium precursors. When $Ti(OBu)_4$ was used as titanium precursor, ethanol was used as solvent for the precursor with a $Ti(OBu)_4$:ethanol molar ratio of 1:10. One molar HCl was added into the mixture until the pH of the mixture was 2.0. When $TiCl_4$ was used as titanium precursor, deionized water was used as the solvent with a $TiCl_4$:water molar ratio of 1:10. Surfactants were dissolved in ethanol and added into the titanium precursor solution slowly (titanium:surfactant:ethanol molar ratio = 1:1:10, 0.5 ml/min). Then the mixture of precursor and surfactants was added into the mixture of deionized water and ethanol slowly (titanium:water:ethanol molar ratio = 1:4:10, 0.5 ml/min). Hydrolysis reaction and polymerization took place in this mixture and a TiO_2 sol was formed. After gelation for 24 h, the gel was dried at 70 °C in an oven until yellow crystal was obtained. After the yellow crystals were calcined in a muffle furnace at a high temperature (500–800 °C), white TiO_2 nanoparticles were obtained.

A XRD scan of the nanoparticles was performed on a D/Max III X-ray diffractometer using Cu Kα radiation (Philips). Fourier transform infrared spectrums (FTIR) were studied using a Bruker Ten 37 FTIR Spectrometer (Bruker Co., Ltd.). The microstructure and morphology of the nanoparticles were observed by a scanning electron microscope, JEOL5900/OXFORD SEM/EDS. The light reflectance property was studied with a Cary50 UV–vis–NIR spectrophotometer (Varian Australia PYT Ltd.).

The photocatalytic activity of prepared TiO_2 nanoparticles was evaluated in fixed film batch reactors using methyl orange (MO) as a model compound. TiO_2 nanoparticles were dispersed in deionized water in a test tube and then treated in an ultrasonic bath (Cole-Parmer Ultrasonic Cleaner, model 08895-16, 100W) for 30 min. Then the suspension was evenly poured onto a 10 cm diameter petri dish. The dishes were dried in an oven and flushed with deionized water until the pH value of the flushing water became neutral and the weight of the dishes was constant after drying at 105 °C. The loading weight of TiO_2 nanoparticles in each petri dish was controlled at 5×10^{-4} g/cm^2. Eighty millilitre of model compound solution was added into the TiO_2 coated dishes. The solution was mixed by using a magnetic stirrer (1.5 cm in length) at a stirring speed of 60 rpm. The reaction was illuminated by a 6 W UV lamp (Blak. Ray UVL 56, wavelength = 365 nm) in a black box. The light intensity was measured by a light intensity meter from Photon Technology International and controlled at 2.5 mW/cm^2 during this study. Solution samples (1 ml/each time) were withdrawn from the fixed film batch reactor for the determination of MO concentration with time and were poured back into the reactor after that. The concentration of MO solution was determined by using a Cary50 UV–vis–NIR spectrophotometer (Varian Australia PYT Ltd.). The wavelength used for the measurement of MO concentration was 465 nm.

The results of blank experiments under similar conditions but without the addition of catalysts indicated that there was a loss of 1–2% solution volume due to the UV irradiation and reactor open to the air but the loss of substrate was negligible. A comparison of the TiO_2 catalyst loading weight before and after photocatalytic reaction suggested that 3–5% of fixed TiO_2 films were sheared out from the Petri dish surface into the solution as suspended particles. For a comparative study of catalyst activity, effect due to this change was not significant.

3. Results and discussion

3.1. SEM images analysis

Fig. 1(a and b) shows the morphologies of TiO_2 nanoparticles obtained from the hydrolysis of $Ti(OBu)_4$ and $TiCl_4$ without using surfactants, respectively. The dimensions of the TiO_2 nanoparticles in Fig. 1(a and b) ranged from ∼100 to ∼200 nm and they are in irregular shapes. In addition, the nanoparticles aggregated and formed large particle blocks. Figs. 2–7 show the different morphologies of TiO_2 nanoparticles obtained with the use of different surfactants and titanium precursors. All the nanoparticles in Figs. 1–7 were calcined at 500 °C.

As shown in Figs. 2–4, uniform spherical and cubic TiO_2 nanoparticles were obtained when DBS and SDS or cellulose was used, respectively. The average dimension of TiO_2 nanoparticles was 250 nm in diameter for spherical particles and 150–300 nm in length for cubic particles. A relatively larger particle size (300 nm) with the use of cellulose would be due to the higher viscosity of the sol. Cellulose contains larger molecular sizes and links than that of the DBS and SDS, which lead to a high viscosity of the TiO_2 sol. The high viscosity of the sol resulted in a larger sol particle size, and this affected its final size.

A striking difference in the shape of TiO_2 nanoparticles were found when $TiCl_4$ was used as a titanium precursor (Figs. 5–7). Uniform ellipse-shape particles with a diameter of about 500 nm were formed when DBS was used, as shown in Fig. 5. Studies suggest that the formation and growth of TiO_2 nanocrystal seeds were determined by the growth competition in [0 0 1] facets and [1 0 1] facets directions [30,31]. In the sol system, the formation of nanoparticles with the lowest surface energy was favoured. In contrast to the case of using $Ti(OBu)_4$, DBS molecules could more easily bind to the anatase [0 0 1] facets of the TiO_2 nucleus because there were fewer organic functional groups surrounding

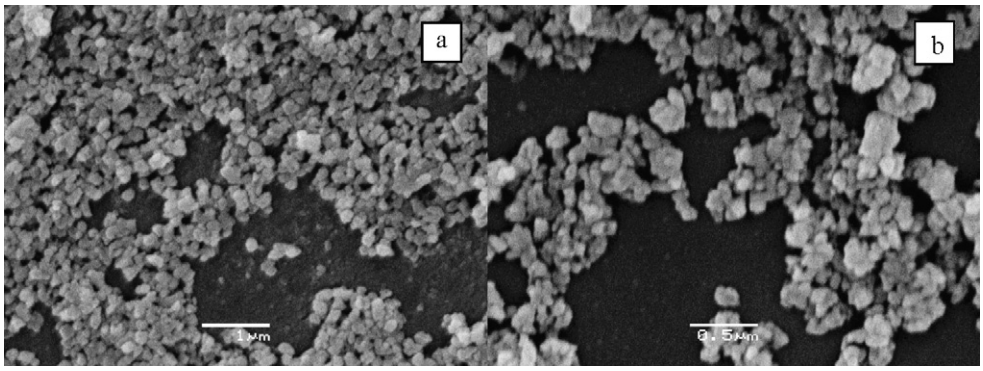

Fig. 1. TiO_2 nanoparticles prepared from $Ti(OBu)_4$ and $TiCl_4$ without using surfactants. (a) $Ti(OBu)_4$ and (b) $TiCl_4$.

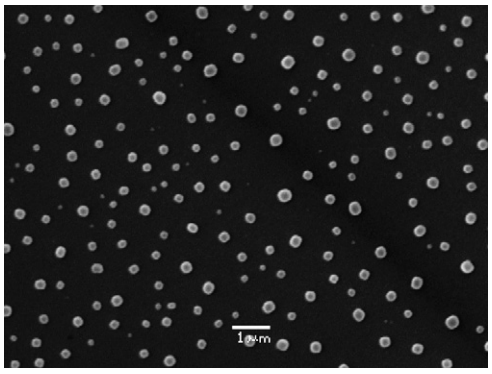

Fig. 2. Nanoparticles shape controlled by DBS from $Ti(OBu)_4$.

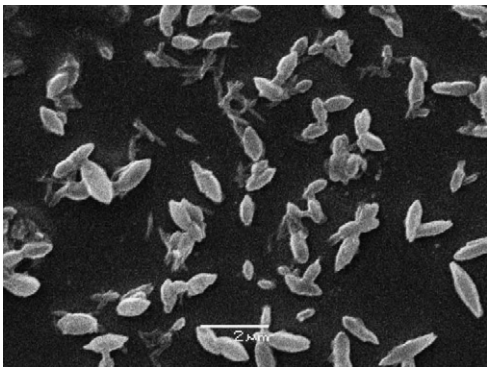

Fig. 5. Nanoparticles shape controlled by DBS prepared from $TiCl_4$.

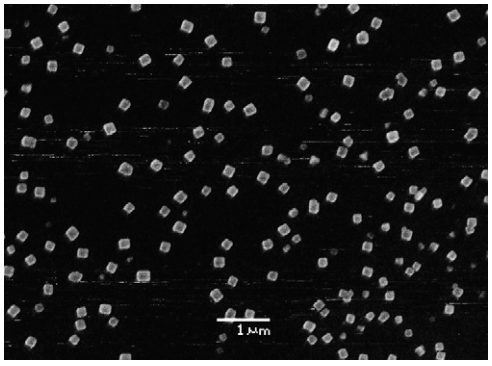

Fig. 3. Nanoparticles shape controlled by SDS from $Ti(OBu)_4$.

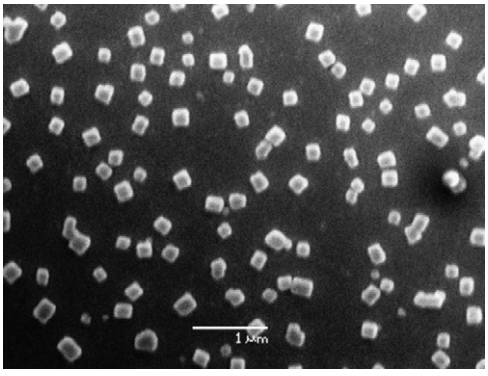

Fig. 6. Nanoparticles shape controlled by SDS prepared from $TiCl_4$.

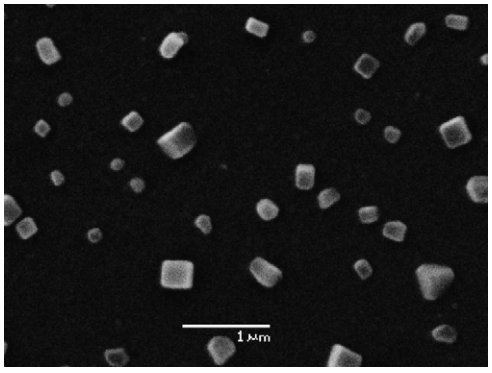

Fig. 4. Nanoparticles shape controlled by cellulose from $Ti(OBu)_4$.

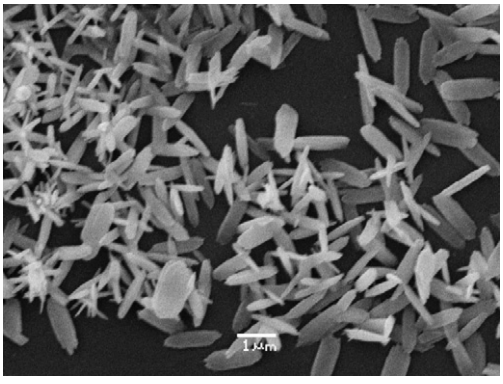

Fig. 7. Nanoparticles shape controlled by cellulose prepared from $TiCl_4$.

the TiO_2 nucleus generated from the $TiCl_4$. When DBS selectively and strongly binds to [0 0 1] facets, the growth rate in this direction is kinetically slowed down. The difference in the growth rates in the two directions of the facets resulted in the ellipse-shape of particles.

Similar to the use of $Ti(OBu)_4$ precursor, cubic nanoparticles, as shown in Fig. 6, were obtained when $TiCl_4$ was used as a titanium precursor with the introduction of SDS. In the case of using $TiCl_4$ precursor, the average dimension of TiO_2 nanoparticles was ~250 nm which was slightly larger than the cubic nanoparticles (150 nm) prepared from $Ti(OBu)_4$. As shown in Fig. 7, short TiO_2 nanorods were observed when cellulose was used. The nanorods had a dimension ranged from 100 to 500 nm in diameter and 200 to 1000 nm in length.

The formation of inorganic nanoparticles in liquid media includes nucleation and monomer growth. The nucleus is characterized by having different shapes and facets, which have different surface energies. The nucleus grows by bonding with other monomers in the media. The nanoparticle growth and the shape formation are related to the crystal surface energy and facets attachment [32]. In the presence of surfactants, surfactants can bind to specific facets of the nucleus and then the nucleus will be coated with a monolayer of surfactant. This monolayer of surfactant can hold the surface energy of the nanocrystal facets and thus control the growth rate from the nucleus to nanoparticles. The attached surfactants will lower the total surface energy of TiO_2 nanocrystals by blocking the high energy facets ([0 0 1] facets of TiO_2) and exposing the low energy facets ([1 0 1] facets of TiO_2). The different shapes and sizes of the nanoparticles in Figs. 2–7 might be related to the different coverage of surfactants for different lengths of molecules, which caused a difference in the growth rate in different directions of exposed nanocrystal facets [31,33].

3.2. X-ray diffraction analysis

Fig. 8(A) shows the X-ray diffraction (XRD) patterns of nanoparticles prepared with different surfactants and calcined at 400 °C. XRD patterns of the prepared TiO_2 nanoparticles indicate the presence of anatase phase (peaks at $2\theta = 25.25°$ [1 0 1] and 48.0°) with a typical anisotropic growth pattern along the [0 0 1] direction. All the nanoparticles consist of anatase as a unique phase. From the XRD patterns, it is known that good crystal was obtained and similar patterns were observed. Surfactants had no significant influence on the phase formation of the nanoparticles. The main reason could be attributed to the fact that the formation of crystal phases is mainly determined by the calcination temperature [34,35].

XRD patterns of TiO_2 nanoparticles shape controlled by SDS and calcined at different temperatures are shown in Fig. 8(B). The degree of crystallinity of TiO_2 was improved with an increase in the calcination temperature which was represented by the higher diffraction intensity. Characteristic peaks of anatase became sharper and narrower when the calcination temperature was increased. Rutile TiO_2 component (peaks at $2\theta = 27.42°$ [1 1 0] and 54.5°) appeared when nanoparticles were calcined at 500 °C. As show in Fig. 8(B) (patterns 2–5), an obvious rutile reflection appeared in the diffraction pattern when the calcination temperature was higher than 500 °C.

3.3. FTIR spectra analysis

Fig. 9(a–c) shows the FTIR spectra of the shape-controlled TiO_2 nanoparticles. Spectrum 1 in Fig. 9(a–c) represents the nanoparticles calcined at 400 °C whereas spectrum 2 represents the nanoparticles dried at 70 °C. A comparison between spectrum 1 and 2 suggests that most of the organic functional groups from surfactants (peaks between 1065 and 3600 cm^{-1}) were decomposed by calcination at 400 °C within 1 h. In the shape-controlled TiO_2 nanoparticles with DBS and SDS, there were some –C–O residuals left in the TiO_2 nanoparticles as indicated in spectrum 1 at 1065 cm^{-1}. The FTIR spectra suggest that there were no attached organic molecules on the nanoparticles after calcination at 400 °C.

3.4. UV–vis spectrum analysis

Shape and size have a significant impact on the optical and electronic properties of nanoparticles [36]. The UV–vis reflectance band edge is a strong function of TiO_2 particle size, which can be attributed to the quantum size effect of semiconductors [37]. Extrapolating the spectral curves to the long-wavelength side provides a measure of the band gap energy of the nanoparticles.

The UV–vis reflectance of TiO_2 nanoparticles is shown in Fig. 10(a and b). An obvious red shift of UV–vis reflectance spectra of shape-controlled TiO_2 nanoparticles (spectra 1, 2 and 3) was observed when compared with the spectra of commercial anatase TiO_2 nanoparticle Degussa P-25 (spectrum 4) and anatase TiO_2 nanoparticles (spectrum 5) obtained without the use of surfactants. Shape-controlled TiO_2 nanoparticles strongly absorbed UV light within a wavelength below 380 nm, while the non-shape controlled anatase TiO_2 nanoparticles absorbed most of the UV light with a lower wavelength (<350 nm). This suggests that the shape-controlled TiO_2 nanoparticles have a lower band gap than the neat anatase TiO_2 nanoparticles and P-25. This is consistent with the observation of Petroski et al. [8].

The lower band gap has a positive effect on the photocatalytic activity because lower source energy is needed to arouse a photocatalytic reaction. The red shift of light reflectance of shape-controlled nanoparticles could be due to a large amount of surface defects on particle surfaces which make the shape-controlled nanoparticles have a higher ability to capture electron-hole pairs. According to the theory of quantum size effect [38,39], Brus [38] suggested that the light absorption of nanoparticles is similar to the absorption by bulk materials when the size of particles is larger than 100 nm. With the morphologies shown in Figs. 2–7, the size difference of the nanoparticles was not the main reason for the lower band gap energy for the shape-controlled TiO_2 nanoparticles. The light absorption happened at higher wavelengths which indicate that lower band gap energy exists in the shape-controlled TiO_2 nanoparticles. Less energy is needed to activate the shape-controlled TiO_2 nanopar-

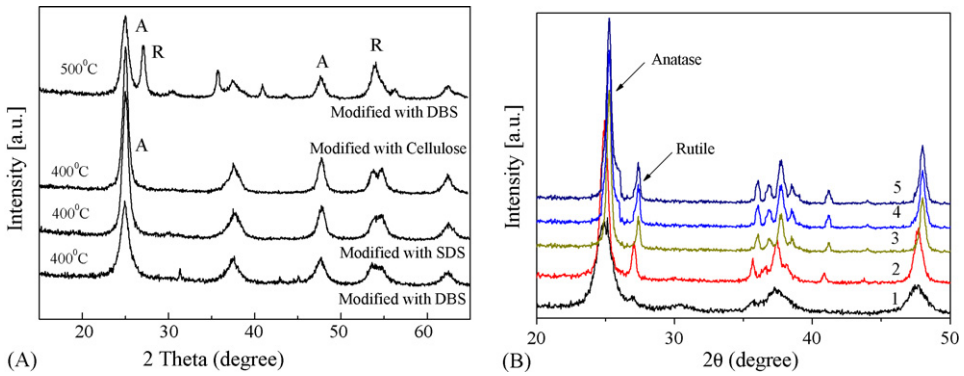

Fig. 8. XRD patterns of shape-controlled TiO_2 nanoparticles. (A) Nanoparticles calcined at 400 and 500 °C. (B) Nanoparticles calcined at different temperatures: (1) 400 °C; (2) 500 °C; (3) 600 °C; (4) 700 °C; (5) 800 °C.

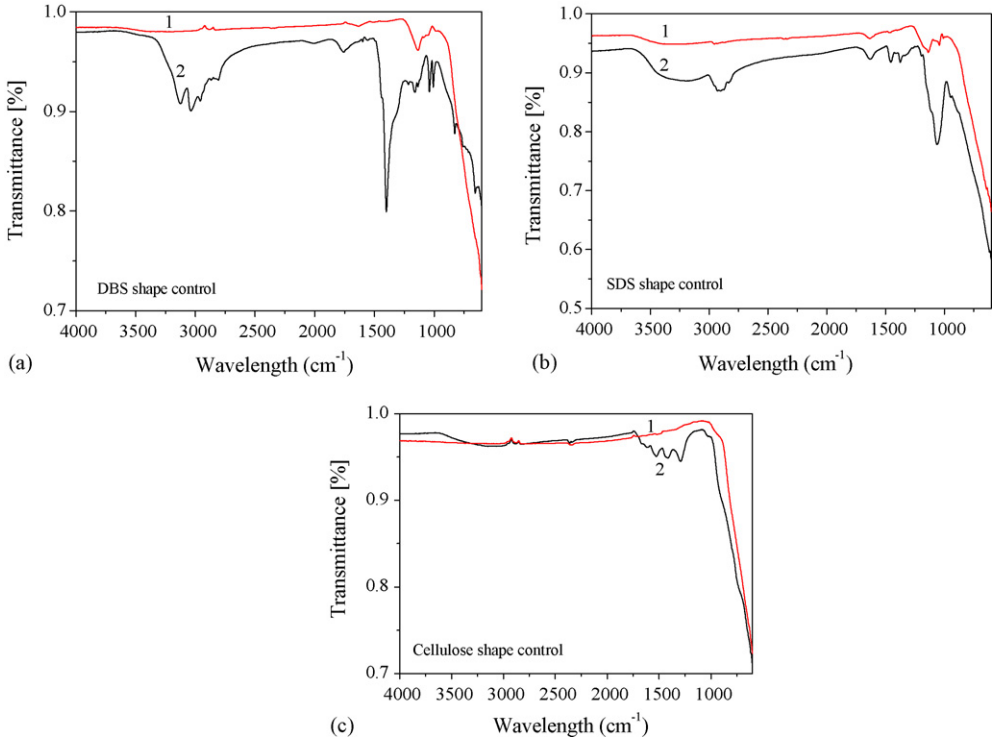

Fig. 9. FTIR spectra of shape-controlled TiO_2 nanoparticles before and after calcination at 400 °C. (a) Nanoparticles with DBS. (b) Nanoparticles with SDS. (c) Nanoparticles with cellulose. (1) Nanoparticles after calcined at 400 °C; (2) nanoparticles dried in oven at 70 °C.

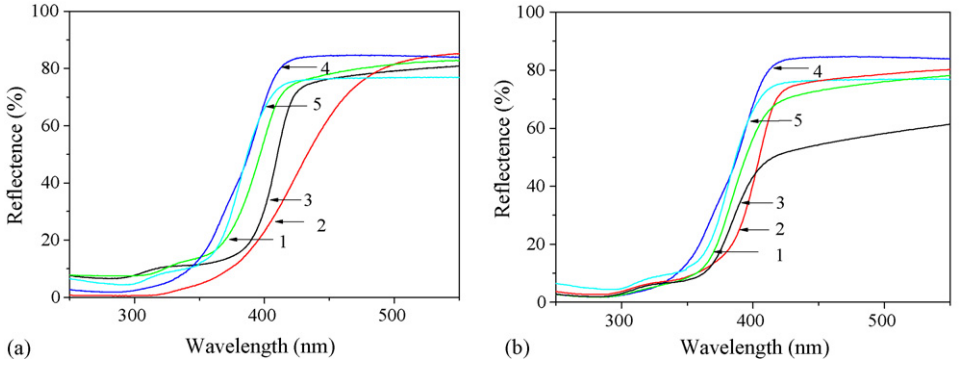

Fig. 10. UV–vis reflectance spectra of the particles dried at 500 °C. (a) Nanoparticles prepared from $Ti(OBu)_4$. (b) Nanoparticles prepared from $TiCl_4$. (1) TiO_2–DBS; (2) TiO_2–SDS; (3) TiO_2–cellulose; (4) P-25; (5) non-shape controlled TiO_2.

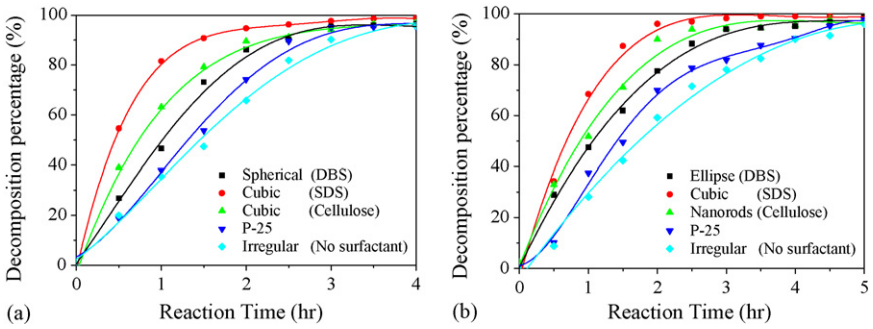

Fig. 11. A comparison on photocatalytic activities of different shape-controlled TiO_2 nanoparticles (initial [MO] = 500 μg/l). (a) Nanoparticles prepared from $Ti(OBu)_4$ and (b) nanoparticles prepared from $TiCl_4$.

ticles to generate excited electron/hole pairs and then induce photocatalytic reactions.

3.5. Photocatalytic activity evaluation

Photocatalytic activity of prepared TiO_2 nanoparticles was evaluated by photocatalytic decomposition of methyl orange (MO) in fixed film batch reactors. The results are shown in Figs. 11 and 12. In comparison with the nanoparticles prepared without using surfactants and P-25, shape-controlled nanoparticles had a higher photocatalytic activity (Fig. 11). The results are consistent with the finding of Wang et al. [11,12] in that photocatalytic activity can be manipulated by adjusting the morphology of TiO_2 photocatalysts. In both cases of using either $Ti(OBu)_4$ or $TiCl_4$ as titanium precursor, cubic TiO_2 nanoparticles shaped by SDS showed the highest photocatalytic activity with MO (Fig. 11). Among the shape-controlled nanoparticles, the highest photocatalytic activity of cubic TiO_2 nanoparticles could be attributed to the smallest particle size and best uniformity in shape as observed in SEM images.

The higher photocatalytic activity of shape- and size-controlled TiO_2 nanoparticles could be explained by their lower band gap energy, as shown in Fig. 10. This is also consistent with the finding of Mele et al. [7] in that an extension of the wavelength range of light absorption of TiO_2 nanoparticles would increase the photocatalytic activity. The size and shape of nanoparticles have significant effects on the optical, electronic and catalytic properties because of changes in surface area, number of active sites and quantum size effect [40]. In addition, the band gap energy is correlated to the photocatalytic activity of nanoparticles [41]. By adjusting the shape and size of nanoparticles, the band gap energy was manipulated, which resulted in changes in photocatalytic activity. Size may not be the only main reason for the higher photocatalytic activity for the shape-controlled nanoparticles. Number of active sites, surface defects, and adsorption properties of shape- and size-controlled TiO_2 nanoparticles, might also be responsible for the higher photocatalytic activity.

According to the XRD analysis, TiO_2 nanoparticles transform from amorphous to anatase and then to rutile, with an increase in the calcination temperature. SDS shape-controlled nanoparticles were calcined at different temperatures (500–800 °C) to investigate the influence of calcination temperature on the photocatalytic activity of TiO_2 nanoparticles. The results obtained from $Ti(OBu)_4$ and $TiCl_4$ precursors are shown in Fig. 12. In both cases, TiO_2 nanoparticles calcined at 600 °C showed the highest photocatalytic activity with the highest decomposition rate of MO. From XRD analysis, it was observed that a considerable rutile phase existed when TiO_2 nanoparticles were calcined at 600 °C (Fig. 8). Although rutile was reported with a lower photocatalytic activity as compared to the anatase phase [36,42], some studies also found the composite of anatase and rutile phase could improve the photocatalytic activity to some degree [43]. The results from our study are in agreement with the previous study [4] in that an optimal anatase/rutile ratio exists for the highest photocatalytic activity.

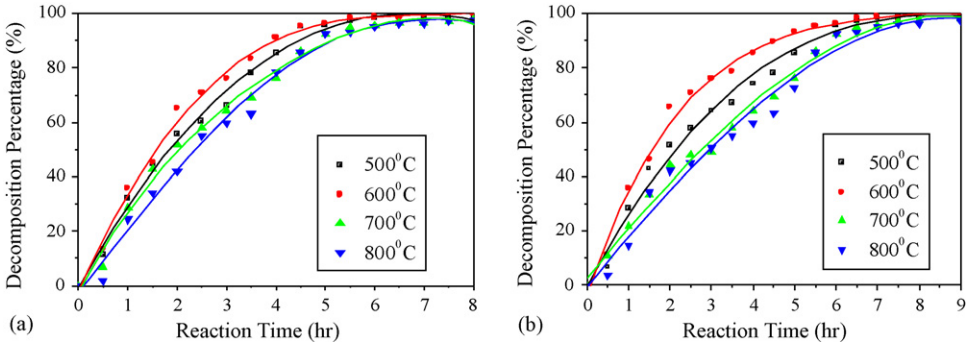

Fig. 12. A comparison of photocatalytic activities of cubic TiO_2 nanoparticles with the introduction of SDS (initial [MO] = 1000 μg/l). (a) Nanoparticles prepared from $Ti(OBu)_4$ and (b) nanoparticles prepared from $TiCl_4$.

Acknowledgement

This study was supported by the Natural Sciences and Engineering Research Council of Canada (NSERC).

References

[1] V.F. Puntes, K.M. Krishnan, A.P. Alivisatos, Science 291 (2001) 2115–2117.
[2] D. Beydoun, R. Amal, S. McEvoy, J. Nanoparticle Res. 1 (1999) 439–458.
[3] X.G. Peng, L. Manna, A.P. Alivisatos, Nature 404 (2000) 59–61.
[4] D.G. Shchukin, D.V. Sviridov, J. Photochem. Photobio. C: Photochem. Rev. 7 (2006) 23–39.
[5] D. Chatterjee, S. Dasgupta, J. Photochem. Photobio. C: Photochem. Rev. 6 (2005) 186–205.
[6] Z.B. Zhang, C.C. Wang, R. Zakaria, J.Y. Ying, J. Phys. Chem. B 102 (1998) 10871–10878.
[7] G. Mele, R. Del Sole, G. Vasapollo, J. Catal. 217 (2003) 334–342.
[8] J.M. Petroski, Z.L. Wang, T.C. Green, J. Phys. Chem. B 102 (1998) 3316–3320.
[9] L. Manna, E.C. Scher, A.P. Alivisatos, J. Am. Chem. Soc. 122 (2000) 12700–12706.
[10] W.G. Lu, P.X. Gao, J.Y. Fang, J. Am. Chem. Soc. 126 (2004) 14816–14821.
[11] X. Wang, J.C. Yu, C. Ho, Langmuir 21 (2005) 2552–2559.
[12] J.C. Yu, X. Wang, X. Fu, Chem. Mater. 16 (2004) 1523–1530.
[13] P.D. Cozzoli, A. Kornowski, H. Welleri, J. Am. Chem. Soc. 125 (2003) 14539–14548.
[14] M.P. Pileni, Nat. Mater. 2 (2003) 145–149.
[15] F.J. Vidal-Iglesias, J. Solla-Gullon, A. Aldaz, Electrochem. Commun. 6 (2004) 1080–1084.
[16] J.H. Lee, I.C. Leu, M.H. Hon, J. Phys. Chem. B 109 (27) (2005) 13056–13059.
[17] A. Mills, N. Elliot, I.P. Parkin, J. Photochem. Photobio. A: Chem. 151 (2002) 171–179.
[18] Y. Bessekhouad, D. Robert, J.-V. Weber, J. Photochem. Photobio. A: Chem. 167 (2004) 69–71.
[19] S.J. Liao, D.G. Huang, D.H. Yu, J. Photochem. Photobio. A: Chem. 168 (2004) 7–13.
[20] A. Piscopo, D. Robert, J.V. Weber, J. Photochem. Photobio. A: Chem. 139 (2001) 253–256.
[21] H. Farzana, V. Elena, H.L. Cooper, J. Photochem. Photobio. A: Chem. 169 (2005) 21–27.
[22] O. Carp, C.L. Huisman, A. Reller, Prog. Solid State Chem. 32 (2004) 33–177.
[23] F. Bosc, A. Ayral, P.A. Albouy, Chem. Mater. 16 (2004) 2208–2214.
[24] P. Yang, D. Zhao, D.I. Margolese, B.F. Chmelka, Nature 396 (1998) 152–154.
[25] L. Wu, J.C. Yu, X.C. Wang, L.Z. Zhang, J. Solid State Chem. 178 (2005) 321–328.
[26] B. Smarsly, D. Grosso, T. Brezesinski, Chem. Mater. 16 (2004) 2948–2952.
[27] S. Ito, T. Takeuchi, T. Katayama, Chem. Mater. 15 (2003) 2824–2832.
[28] D.M. Antonelli, J.Y. Ying, Angew. Chem. Int. Ed. English 34 (2003) 2014–2017, 828.
[29] M. Alvaro, C. Aprile, M. Benitez, J. Phys. Chem. B 110 (2005) 6661–6665.
[30] R.L. Penn, J.F. Banfield, Geochim. Cosmichim. Acta 63 (1999) 1549–1552.
[31] H.T. Liu, A.P. Alivisatos, Nano Lett. 4 (12) (2004) 2397–2401.
[32] Y.D. Yin, A.P. Alivisatos, Nature 29 (2005) 437–439.
[33] R.L. Penn, J.F. Banfield, Science 281 (1998) 969–971.
[34] D. Beydoun, R. Amal, Mater. Sci. Eng. B 94 (2002) 71–81.
[35] A. Fujishima, T.N. Rao, D.A. Tryk, Electrochim. Acta 45 (2000) 4683–4690.
[36] U. Diebold, Surf. Sci. Rep. 48 (2003) 53–229.
[37] J.F. Banfield, Nanoparticles and the Environment, Mineralogical Society of America, Washington, DC, 2001.
[38] L. Brus, J. Phys. Chem. 90 (1986) 2555–2560.
[39] J.W. Halley, M. Kozlowski, N. Tit, Surf. Sci. 256 (1991) 397–408.
[40] I.A. Banerjee, L.T. Yu, H. Matsui, PNAS 100 (25) (2003) 14678–14682.
[41] L. Manna, E.C. Scher, A.P. Alivisatos, J. Cluster Sci. 13 (4) (2002) 521–532.
[42] T. Ivanova, A. Harizanova, M. Surtchev, Solar Energy Mater. Solar Cells 76 (2000) 591–598.
[43] R.E. Tanner, Y. Liang, Surf. Sci. 506 (2002) 251–256.